

AN ABSTRACT OF THE THESIS OF

Ramsey Tachella for the degree of Master of Science in Robotics presented on
May 11, 2016.

Title: Design and Development of a Salticid Inspired Jumping Robot

Abstract approved: _____

Ross Hatton

The ability to jump allows small robots to traverse rough terrain, clear large obstacles, and quickly reach elevated locations. These abilities have applications in a variety of areas such as, search and rescue, environmental monitoring, and urban warfare. The primary focus in current state-of-the-art jumping robots has been on jumping as high or far as possible, with little focus on how to change the prelaunch dynamics to accomplish different trajectories. This lack of variety limits the utility of jumping robots by reducing their effective workspace. To solve this problem, we explored the jumping behavior of the Salticid family of jumping spiders. Salticid spiders are able to change their leg geometry and use their front legs to channel jump energy into a vaulting motion. Vaulting allows the spider to achieve flatter trajectories than are possible by extension of the rear legs alone. We mapped the spiders jumping mechanism onto a four-bar linkage to develop a model for the spiders jumping mechanics. This model is then used to develop a robot that is able to effectively mimic the spider's jumping behavior.

©Copyright by Ramsey Tachella
May 11, 2016
All Rights Reserved

Design and Development of a Salticid Inspired Jumping Robot

by

Ramsey Tachella

A THESIS

submitted to

Oregon State University

in partial fulfillment of
the requirements for the
degree of

Master of Science

Presented May 11, 2016
Commencement June 2017

Master of Science thesis of Ramsey Tachella presented on May 11, 2016.

APPROVED:

Major Professor, representing Robotics

Head of the School of Mechanical Industrial and Manufacturing Engineering

Dean of the Graduate School

I understand that my thesis will become part of the permanent collection of Oregon State University libraries. My signature below authorizes release of my thesis to any reader upon request.

Ramsey Tachella, Author

ACKNOWLEDGEMENTS

I would like to thank my colleagues at the Laboratory for Robotics and Applied Mechanics for their help and guidance, my family for always being there for me, and my fiancé Claire for all of her love and support.

TABLE OF CONTENTS

	<u>Page</u>
1 Introduction	1
1.1 Motivation	2
1.2 Biological Inspiration	3
1.3 Jumping Robots	6
2 Modeling	9
2.1 Spider Model	10
2.2 Jumping Behavior	13
2.3 Proof-of-Concept Model	16
3 Explored Designs	19
3.1 Design Criteria	19
3.2 Hydraulic Jumper	20
3.3 Screw Spider	21
4 Final Design	23
4.1 Jumping Mechanism	23
4.2 Motor and Controller	29
4.3 Mass Concentration	31
4.4 Vaulting Mechanism	33
5 Results and Discussion	36
5.1 Video Results	36
5.2 Motion Capture	39
6 Conclusion	43
Bibliography	44

LIST OF FIGURES

<u>Figure</u>		<u>Page</u>
1.1	Final robot developed in this thesis.	2
1.2	Image of Salticid spider lifting its first and second legs as it prepares to preform a jump.	5
1.3	Sequential image of <i>Maratus</i> performing a jump.	5
1.4	Current state-of-the-art jumping robots.	7
2.1	Reaction force for the aiming jump at the instant the spring released.	9
2.2	Reaction forces for the vaulting jump at the instant the spring released.	10
2.3	Simplified model of Salticid jumping mechanics developed by Hill.	10
2.4	Four-bar model of spider jumping mechanics developed by Faraji et.al.	11
2.5	Salticid spider performing jump with drag-line attached.	12
2.6	Robot behavior as it performs aiming and vaulting jumps.	13
2.7	Jumping behavior for determined non-dimensional stiffness.	15
2.8	Predicted trajectory results from ballistic kinematics calculation.	16
2.9	Proof-of-concept model developed to verify aiming and vaulting jumping behavior.	17
2.10	Proof-of-concept model successfully performing aiming and vaulting jump.	18
3.1	4-bar model of mechanism before jump.	19
3.2	Leadscrew inspired design concept.	21
4.1	Escapement cam attached to four-bar linkage.	24
4.2	Exploitation of cam's geometry to determine forces acting on the cam's profile.	28
4.3	Implementation of microcontroller and motor shield.	30

LIST OF FIGURES (Continued)

<u>Figure</u>		<u>Page</u>
4.4	CAD model of robot's main body.	32
4.5	Hard stops to constrain the rotation of the robots front legs.	35
5.1	Representation of final and initial launch angles for the vaulting jump.	37
5.2	Frame by frame shots detailing the robot's behavior as it performs different jumps.	38
5.3	Averaged results from motion capture data for the aiming and vaulting jumps.	39
5.4	Motion capture data from individual iterations of the aiming and vaulting jumps.	40

LIST OF TABLES

<u>Table</u>	<u>Page</u>
1.1 State-of-the-art miniature jumping robot mechanisms.	8
4.1 Weight distribution for jumping robot.	32

Chapter 1: Introduction

The goal of this project is to develop a novel, biologically inspired, jumping robot with the ability to modulate its prelaunch geometry to accomplish different jumping behaviors. Inspiration for this project stems from previous research conducted by Faraji et.al [1], that investigated the creation of a jumping mechanism based on the dynamics of Salticid spiders. Previous research preformed by Hill [2], determined that Salticid spiders are able to modulate their jumping behavior based on leg configuration. Faraji et.al expanded on this research, to develop a model that utilizes a non-dimensional stiffness to characterize jumping behavior. Results from the model, show that two types of jumping behavior can be achieved, based on the relative angle between the legs. To advance this research into practical applications, I developed a novel energy storage mechanism that effectively shifted the center of mass from the point of actuation to the center of the main body. To facilitate the jump motion, I developed non-slip feet for the robot that are able to rotate, but not translate during the jump motion. Furthermore, I developed a pivot mechanism that allows the robot to vault about its' center of mass during the jump motion. The robot I developed in this thesis is shown in Figure 1.1.



Figure 1.1: Final robot developed in this thesis.

This chapter will provide the motivation for this project, background on current jumping robots, and their biological inspiration. Chapter 2 will detail the methods used to model the behavior of the robot. Chapters 3 and 4 will detail the design process. Finally, Chapters 5 and 6 will discuss results obtained and provide incite into the next step of the project, respectively.

1.1 Motivation

Jumping allows small robots to traverse rough terrain, clear large obstacles, and quickly reach elevated locations. This behavior is not possible for other types of terrestrial locomotion [3–6]. These abilities have applications in a variety of areas such as, search and rescue, environmental monitoring, military surveillance, and urban

warfare [7, 8]. The primary focus in current state-of-the-art jumping robots has been on jumping as high or far as possible, with little focus on how to change the prelaunch-phase jump dynamics to accomplish different trajectories [1]. This lack of variety limits the utility of jumping robots by reducing their effective workspace. If a robot’s primary design is to jump high as possible, it may have the required energy to reach a long distance, but that energy is wasted on unnecessary height. Extra height also limits a robot’s ability to reach an object when there is an obstruction over the target. Our robot will overcome these shortcomings by focusing on exploiting leg geometry to feature different jumping behaviors. This novel jumping behavior allows our robot to execute the typical jumps behavior seen in many of today’s robots, and to utilize its front legs as a vaulting mechanism to channel stored energy into a flatter trajectory. For the purpose of conciseness, the two jumping behaviors exhibited by our robot will be referred to as an aiming jump for standard jumping behavior, and a vaulting jump when the front legs channel energy to achieve flatter trajectories.

1.2 Biological Inspiration

Biological organisms utilize jumping for a variety of functions. Locusts use jumping for primary locomotion, fleas as a means of overcoming large obstacles, and spiders for prey capture. Biologically evolved methods provide good inspiration for modeling, developing, and setting benchmarks for a variety of walking, grasping and jumping robots [9, 10].

Much of the biologically inspired research done in development of jumping robots

has focused on propulsion mechanisms [11–13]. This is due to the high acceleration required for a robot to jump. Utilizing mechanisms adapted from biological organisms such as, locusts [14], frogs [15], and fleas [16] has resulted in a variety of powerful propulsion mechanisms. Since the propulsion system has been studied extensively, we chose to adapt an existing design for our robot and instead focus on jump mechanics.

The biological inspiration of our research is the Salticid family of jumping spiders. Salticid spiders are able to modulate their jumping behavior through prelaunch geometry, propulsion power, and a drag line to effectively capture prey, navigate rough terrain, and avoid predators [2]. The jumping mechanics of Salticid spiders were first explored by Parry and Brown [17]. Through their study of *Sitticus pubescens*, they determined the basic mechanics these spiders use to jump. Their study found *S. pubescens* only utilize two pairs of legs when jumping. Their rearmost, or forth pair of legs provide power, while the third pair serve to guide the jump. The first and second pair of legs are held off the ground and do not have any effect on jumping motion, shown in Figure 1.2. Further research by Hill [2] on the species *Phidippus princeps* determined Salticids utilize haemocoelic blood pressure to hydraulically straighten their rear legs and generate power for jumps. Variation of this pressure, along with the configuration of the front and rear legs, allows *P. princeps* to change the direction and magnitude of their take-off velocity, which allows for different ballistic flight paths. *Phidippus princeps*' are able to perform accurate jumps at horizontal distances of up to 10 cm, which is 20 times their body length.

Research performed by Parry [17] and Hill [2] has examined the jumping behavior of only two genera, *Sitticus* and *Phidippus*. Most Salticids utilize internal pressure to



Figure 1.2: Image of Salticid spider lifting its first and second legs as it prepares to preform a jump [2].

power their jumps, which is evident by the extension of spines on the spider's legs, and lack of an external muscle structure [17, 18]. Some genera of Salticids however, transmit this power through different appendages. Recent research performed by Otto and Hill [18, 19] on the genus *Maratus*, show this genera rely on the extension and rotation of their third pair of legs as the primary method to power their jumps, shown in Figure 1.3. This behavior is apparent since the third pair of legs is longer than the fourth, and experiences a greater compression before the spider performs

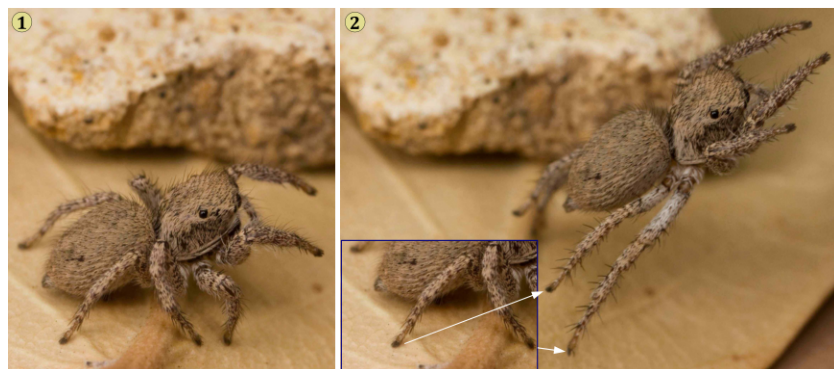


Figure 1.3: Sequential image of *Maratus* performing a jump [18].

a jump [18]. Although the jumping mechanics of *Maratus* has not been studied as extensively as *Sitticus* or *Phidippus*, it is thought that this adaptation allows these spiders to perform vertical jumps and is a more efficient configuration when jumping down on prey from ledges [19]. The robot developed in this thesis will draw on inspiration from the studies performed by Parry [17] and Hill [2] on spiders found in the *Sitticus* and *Phidippus* genera.

1.3 Jumping Robots

Jumping robots are typically distinguished by two classes: regenerative hopping and pause and leap [3]. The regenerative hopping class, contains robots that use successive jumping as a means of locomotion. Once the jumping motion is complete, the robot needs to be ready to immediately jump again. These robots are typically large and, require high speed and high force actuators. The pause and leap class defines robots that are typically smaller and utilize jumping as a means to clear obstacles. Since these robots do not need to perform immediate successive jumps, their jumping mechanisms charge slowly, resulting in lower power requirements [16, 20]. Pause and leap robots implement mechanisms that slowly charge elastic elements, such as, springs or rubber bands to store energy [4, 21]. The robot developed in this thesis will focus on proving ability to modulate its jumping behavior before launch, which does not require immediate successive jumps, so it is in the pause and leap class.

The techniques required for pause and leap jumping have been implemented through a variety of catapult mechanism types [16], shown in Figure 1.4 and Ta-

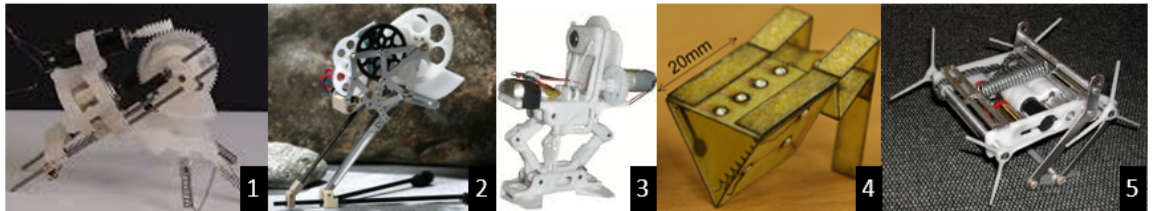


Figure 1.4: Current state-of-the-art jumping robots. Robot names, from left to right: Grillo, 7g Jumping Robot, Miniature Jumping Robot, Flea Catapult, Mini-Whegs

ble 1.1. The Grillo [22] and 7g Jumping Robot [14] utilize a spiral cam mechanism to slowly charge a spring until an escapement point on the cam is reached. Once the escapement point is reached, the energy stored in the spring is released. The Miniature Jumping Robot [8] implements a one-way bearing connected to a cable that drives a scissor type mechanism. Compression of this mechanism stores energy in two torsional springs. Once rotation of the bearing reaches a certain point, the cable uncoils, and the spring’s energy is released. The flea inspired robot [16] utilizes the phase transition of a shape memory alloy spring, to store energy. The spring’s energy is then stored by a trigger mechanism, which releases when activated. Mini-Whegs [23] utilizes a notched gear to drive a four-bar mechanism which compresses a linear spring. Once the notched section of the gear is reached, the energy stored in the spring is released. All of the aforementioned robots feature effective energy storage methods, however they are only able to change their take-off dynamics through robot reconstruction.

Both the Grillo and 7g Jumping Robot are able to modify their take-off trajectory through changes of their feet or legs. These methods require significant changes to the robot making them impractical for real-world applications. Another concept being

Table 1.1: State-of-the-art miniature jumping robot mechanisms.

Robot	Release Mechanism	Energy Storage
Grillo	Escapement cam	Linear spring
7g Jumping Robot	Escapement cam	Torsional spring
Miniature Jumping Robot	One-way bearing	Two torsional springs
Flea Catapult	Trigger	Linear Spring
Mini-Whegs	Notched Gear	Linear spring

developed by Kosa [24] is to change jump dynamics by adding wings to the robot that extend after it has reached its peak jump height. The wings interrupt the initial ballistic trajectory and allow the robot to glide, increasing the distance it travels. While this method changes the dynamics of the robots jump, low and flat trajectories are not possible. With slight modification the robot developed here will be able to change its jumping behavior on demand to achieve low, flat trajectories.

Chapter 2: Modeling

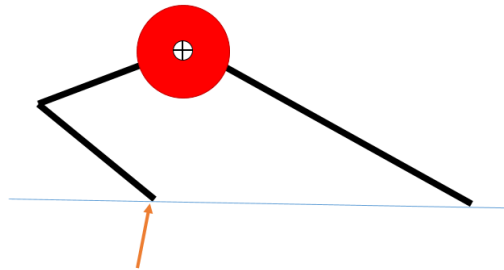


Figure 2.1: Reaction force for the aiming jump at the instant the spring released.

For this thesis we will explore two types of jumping behavior: the aiming jump and the vaulting jump. The jump behavior is determined based on leg configuration before take-off. To perform an aiming jump, the robot will position its legs so the net reaction force applied will point directly through the center of mass, shown in Figure 2.1. This position results in no force being applied to the front legs and causes the robot to follow a ballistic trajectory, along the direction of the reaction force vector. To perform a vaulting jump, the robot positions its legs so the net reaction force will point behind the center of mass, creating a moment around the robot's body, Shown in Figure 2.2. This moment results in redirection of jumping force into the front legs. Once the force is transmitted to the front legs, the resulting force vector remains perpendicular to the front legs until the force is removed and the robot begins to leave the ground. The resulting jump is flatter than an aiming jump and the robot travels a greater distance [1]. This chapter details the methods used to develop a

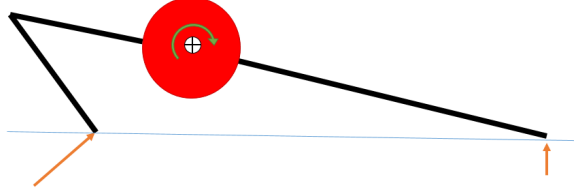


Figure 2.2: Reaction forces for the vaulting jump at the instant the spring released.

mechanical model for the robot. First, the structure of the spider will be explored, and a analytical model will be formed. Next, relationships will be developed that allow for the characterization of the types of jumps the robot will perform. Finally, design criteria will be determined and a proof-of-concept model will be developed.

2.1 Spider Model

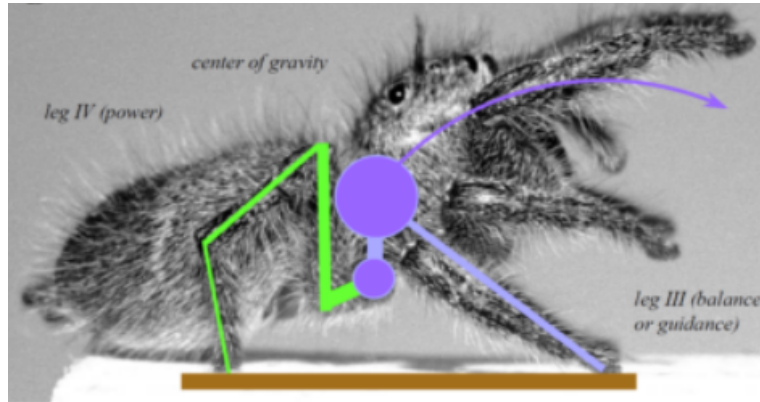


Figure 2.3: Simplified model of Salticid jumping mechanics developed by Hill [2].

Figure 2.3 shows the jumping model developed by Hill [2]. This model details the essential components of the spider that are required for it to perform a jump. Leg *IV*

provides power for the spider to jump. The large circle in the center of the spider's body shows the center of gravity. Leg *III* is used to stabilize or guide the spider depending on the type of jump it performs [2]. A simplified model was developed by Faraji et.al [1], which mapped Hill's model onto a four bar linkage, shown in Figure 2.4. Decomposition into a four-bar linkage allows for simplified dynamics, while preserving the overall jumping motion of the spider.

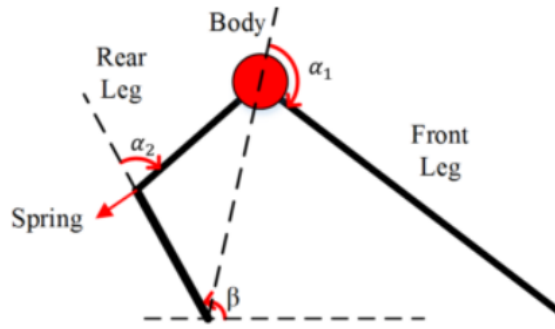


Figure 2.4: Four-bar model of spider jumping mechanics developed by Faraji et.al [1].

The most distinguishable feature of the new model is the rear leg. The rear leg is constructed of two links, a single actuation joint, and is mounted directly to the center of mass. Constructing the leg using two links is similar to Hills model, since its only function during a jump is to transmit actuation force to the ground. The two links feature three pin joints, and transmit magnitude and direction of the foot's reaction force directly through the main body. In Hill's model the rear leg is attached with a rigid link below the center of mass, which is different than the attachment in our model. The attachment point of the rear leg in Hill's model results in a moment being applied to the spider's body before it leaves the ground. On the physical spider this attachment position causes it to rotate backward [2], shown in Figure 2.5. The spider

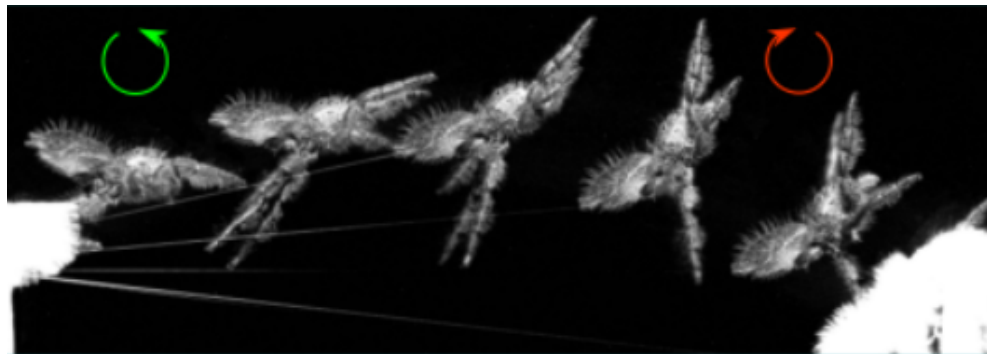


Figure 2.5: Salticid spider performing jump with drag-line attached. The green arrow represents the spiders rotation as it leaves the ground. The red arrow shows the rotation experienced as the spider uses its drag-line to modify its trajectory [2].

then uses its drag-line to modify its trajectory and counteract the rotation, which is shown by the green arrow in the image. Our robot does not have the capability of using a drag-line to modify its trajectory, so the rear leg is attached at the center of mass to reduce rotation during flight. Since the link that attaches the rear leg in Hill’s model is rigid, the resulting system will exhibit the same dynamics during the jumping motion.

2.2 Jumping Behavior

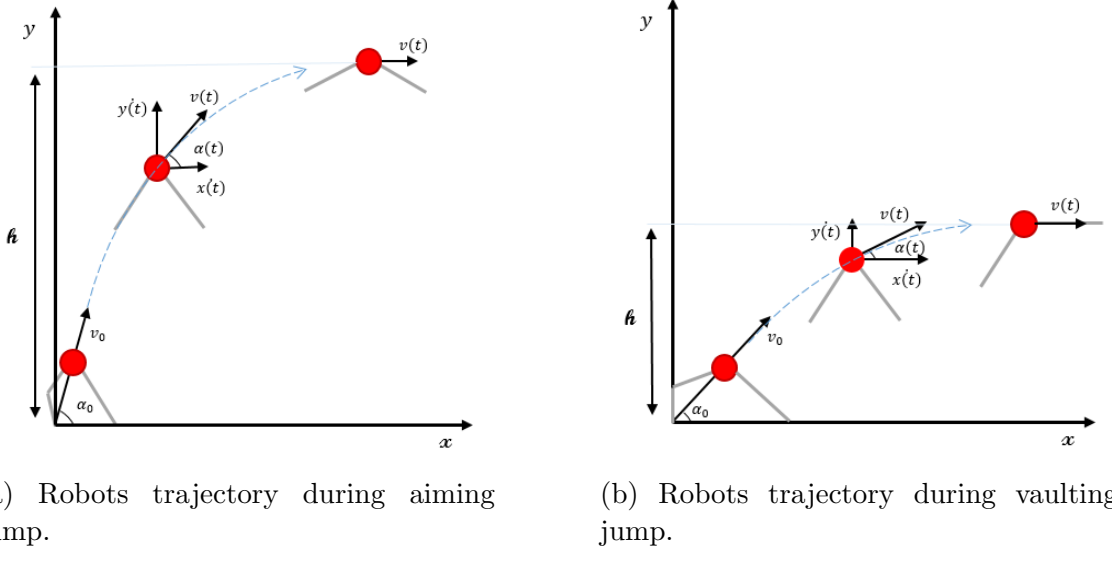


Figure 2.6: Robot behavior as it performs aiming and vaulting jumps.

We adopted a ballistic kinematics model developed by Kovač [11] to model the robot's trajectory during the flight phase of the aiming and vaulting jumps. Models used for the two jumps are shown in Figure 2.6. The resulting force balance is shown in Equation 2.1.

$$\begin{aligned}\ddot{x}(t) &= -\frac{1}{2m}\rho Ac_d \cos\left(\arctan\left(\frac{\dot{y}(t)}{\dot{x}(t)}\right)\right) (\dot{x}(t)^2 + \dot{y}(t)^2) \\ \ddot{y}(t) &= -\frac{1}{2m} \left[2mg + \rho Ac_d \sin\left(\arctan\left(\frac{\dot{y}(t)}{\dot{x}(t)}\right)\right) (\dot{x}(t)^2 + \dot{y}(t)^2) \right]\end{aligned}\quad (2.1)$$

The result is a coupled, second-order, nonlinear, differential equation, where m is the total mass of the robot, ρ is the density of air, A is the surface area of the robot, g is gravity, and c_d is the coefficient for drag. The initial conditions used to model the

system are as follows:

$$\begin{aligned}\dot{x}(0) &= \cos(\alpha_0)v_0 \\ \dot{y}(0) &= \sin(\alpha_0)v_0 \\ x(0) &= 0 \\ y(0) &= 0\end{aligned}\tag{2.2}$$

where α_0 is the initial angle of the jump, and v_0 is the magnitude of the velocity just before the robot leaves the ground. The first and second initial conditions in Equation 2.2, state the robot has no initial velocity before it performs the jump. The third and forth initial conditions, state the robot begins its jump at the origin of the coordinate system. This constraint allows the system position to begin at 0 and creates a trivial baseline to determine the height and distance of the jump.

We developed an energy balance, shown in Equation 2.3, to relate the energy stored in the spring to the initial velocity v_0 of the jump,

$$\frac{1}{2}k\theta = \frac{1}{2}mv_0^2\tag{2.3}$$

where k is the spring constant for the actuator and θ is the angle that will be swept by the rear leg as it moves from its compressed state to full extension. This relationship states that all of the energy stored in the spring will be directly converted to kinetic energy, and does not account for all losses the system will experience.

Both aiming and vaulting behaviors had to be considered to determine the direction of the robots take-off velocity α_0 . Direction is determined using the front leg angle and non-dimensional stiffness relationship developed by Faraji et.al [1], shown

in Equation 2.4,

$$\rho = \frac{k}{m} \cdot \frac{L_1+L_2}{g} \quad (2.4)$$

where L_1 and L_2 are the lengths of the rear leg segments. After the non-dimensional stiffness was obtained α_0 is determined from the leg geometry and the plot shown in Figure 2.7.

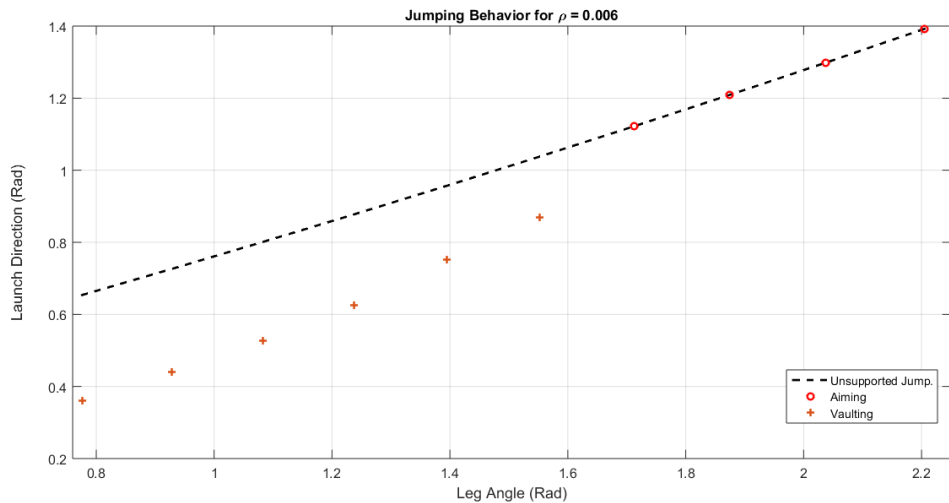


Figure 2.7: Jumping behavior for determined non-dimensional stiffness [1].

Results from the ballistic calculations are shown in Figure 2.8. The predicted height and distance for the aiming jump with a launch angle of 75 degrees are 46.6 cm and 49.3 cm, respectively. The predicted height and distance for the vaulting jump with a launch angle of 49.5 degrees are 28.4 cm and 98.3 cm, respectively.

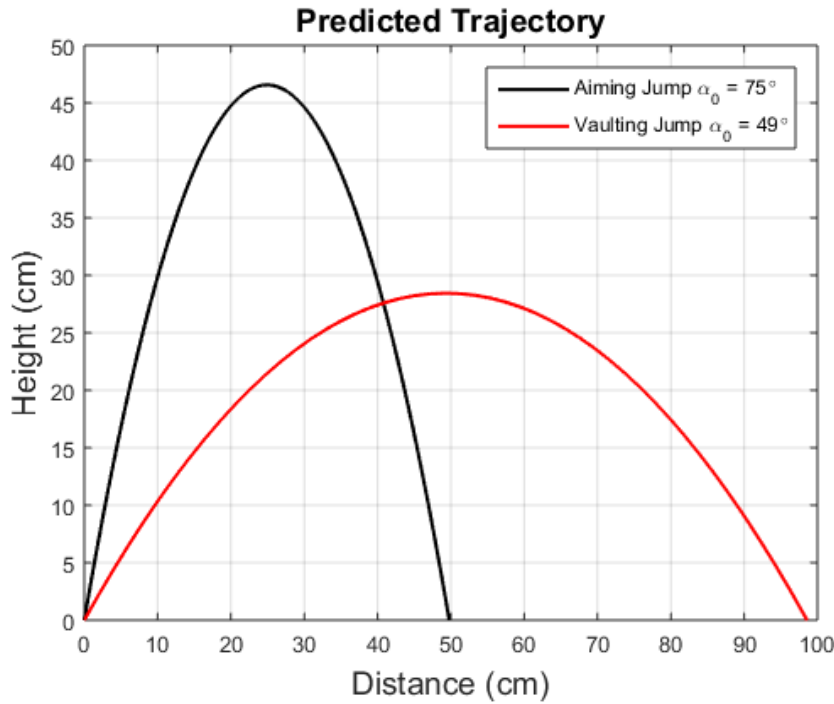


Figure 2.8: Predicted trajectory results from ballistic kinematics calculation.

2.3 Proof-of-Concept Model

We created a mechanical proof-of-concept model to demonstrate the aiming and vaulting motions on a physical system, shown in Figure 2.9. This model consists of four primary parts: front legs, rear legs, main body, and leg stoppers. The front and rear legs are of equal length (165mm) and 3D printed with ABS plastic. The main columns of the legs feature a c-channel design, in order to save weight and provide necessary strength. The three ground contact points on the legs have small extruded spikes to prevent slipping during the jumping motion. The front legs are fixed to-

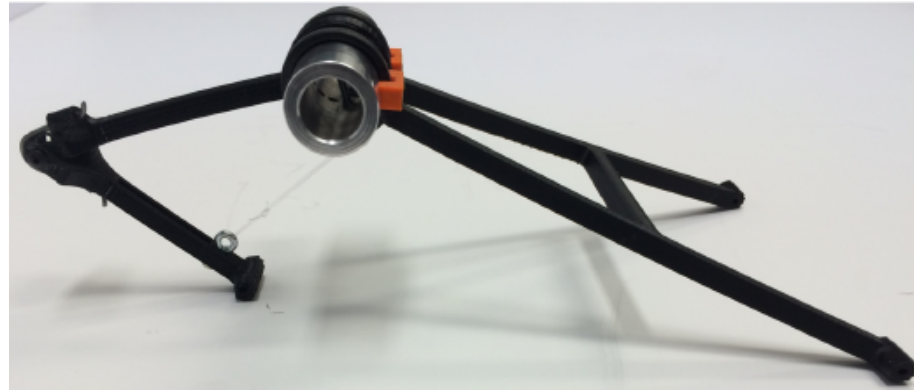


Figure 2.9: Proof-of-concept model developed to verify aiming and vaulting jumping behavior.

gether with a cross brace to ensure even tracking and increased rigidity. The rear leg features a joint at the midpoint, which is fitted with a torsional spring to actuate the jumping motion. The spring is loaded manually, and secured with fishing line using two eyebolts located at opposite ends of the rear leg. To actuate the jumping motion, the fishing line is cut, which releases energy stored in the spring. The main body of the mechanism is constructed using a single hollow tube of aluminum. The interface of plastic legs with aluminum creates a low friction surface, allowing the front legs to rotate, while providing enough weight for the center of mass to remain concentric with the main body. The lateral center of the main body features twelve tapped holes that are drilled at 30 degree increments around its circumference. These holes allow the angle between front and rear legs to be adjusted by removing the eyebolt at the top of the rear leg, and rotating the leg around the body. The leg stoppers are set at a fixed position on the main body and ensure the front legs are at the proper angle before the jump is executed. The photos in Figure 2.10 show that the proof-of-concept



Figure 2.10: Proof-of-concept model successfully performing aiming jump (top) and vaulting jump (bottom).

model is able to effectively complete both the aiming and vaulting jumps. Validation of the model allows for development of a more complicated mechanism that is able to jump remotely.

Chapter 3: Explored Designs

3.1 Design Criteria

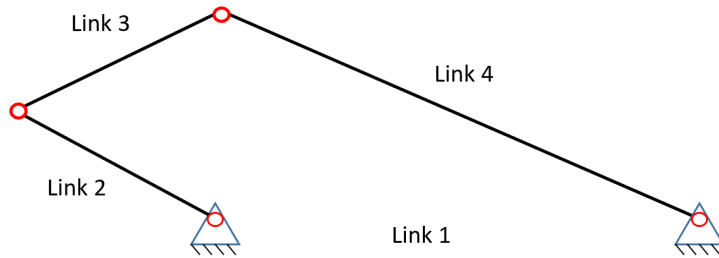


Figure 3.1: 4-bar model of mechanism before jump.

After developing an effective model, design criteria for the final product were identified. Shown in Figure 3.1 is the four-bar linkage the robot will model. The linkage consists of four pin joints with a torsional actuator located between links 2 and 3. With the essential framework laid out, design criteria were developed as follows:

- An actuator located between links 2 and 3 to initiate jumping motion
- A wireless controller that allows for the robot to be controlled remotely
- Adjustable angular constraints between links 3 and 4 that allow for adjustments of jump characteristics

- A friction free joint between links 3 and 4 to allow front legs to passively rotate during the jumping motions
- Non-slip feet that rotate to simulate a pin joint, and ensure proper force transmission during the preflight jumping motion
- A center of mass concentrated between links 3 and 4 to reduce rotation while in flight

3.2 Hydraulic Jumper

To initiate their jumps, spiders utilize muscles inside their body to compress a fluid sack and create hydraulic pressure. The hydraulic pressure is then channeled into deflated sacks in the rear legs, causing them to expand. Expansion of these sacks extends the rear leg, which provides power needed to jump. This was the first method explored to develop this robot.

To mimic the behavior of a spider, a small linear hydraulic actuator was placed between links 2 and 3 to extend the rear leg. Fluid for the system was stored in a bladder, which was placed inside the robot's body and attached to the actuator. Then the bladder was pressurized through the use of two charged linear springs that simultaneously extend and compress the bladder.

There are multiple reasons why this method was not adopted, when compared to the selected actuator. First, a mechanism would need to be designed that could perform the same linear motion required to charge a torsional spring, but with the

added weight of a hydraulic system. Second, the addition of a hydraulic cylinder between links 2 and 3 would significantly move the center of gravity behind the main body, resulting in a change in system dynamics. Third, it would be difficult to implement a resetting system without further affecting the center of mass.

3.3 Screw Spider

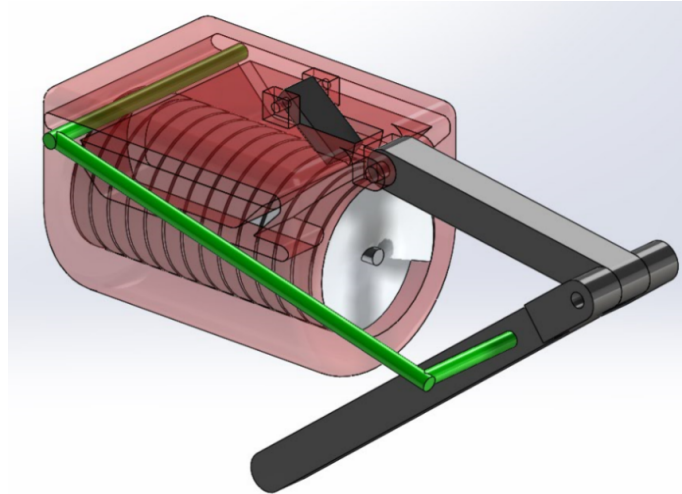


Figure 3.2: Leadscrew inspired design concept.

The leadscrew inspired design concept is shown in Figure 3.2. The jumping mechanism is actuated by using a torsional spring, which is compressed by moving a follower down the leadscrew. The follower's path is defined by a trapezoidal groove cut into the side of the main body. When the follower reaches the front of the body, it moves up the ramp until it is no longer in contact with the screw releasing the spring's energy. The black cam mechanism, shown at the top rear of the body, is spring loaded

and serves to force the follower into the screw mechanism after a jump is performed. To power this mechanism a constant speed DC motor is attached to the front of the body.

The screw mechanism has many useful attributes, however multiple issues removed it from being functional for our final design. The first problem is a large moment being applied at the follower, which would likely cause binding since the bar linking the follower to the rear leg can only be on one side of the mechanism. The binding issue could be solved by placing the follower in a channel and adding two thrust bearings, but additional issues prevented further exploration. The second issue is the complications of manufacturing. The complex nature of the screw housing indicates a need for 3D printing. However, the internal attachment of the follower guide requires a sturdier material than available 3D printed plastics can provide. The third problem with this design is the motor torque required to actuate the leadscrew is too high to use a lightweight motor. A lightweight motor is necessary to prevent a shift in the center of mass to the front of the robot.

Chapter 4: Final Design

Many factors were considered to complete the mechanical design for this robot. The first consideration is the propulsion mechanism. This required consideration of how to properly balance the power to weight ratio and provide enough power to compress the spring, while insuring the robot is still light enough to leave the ground. Second, a controller and power supply were selected. Third, we determine how to keep the mass concentrated at the center of the main body, to reduce rotation. Finally, we determine how to modulate jumping behavior from the aiming to vaulting jumps, and how to ensure the robot is able to pivot about the front legs without impeding the jumping motion. All of these factors are presented sequentially in this section along with the final design.

4.1 Jumping Mechanism

To develop a jumping mechanism, several design concepts were explored, which are detailed in Chapter 3. The mechanism chosen for this project is adopted from work done by Kovač, Carabiener, and Scarfogliero [5, 11, 25] and is shown in Figure 4.1. The mechanism is an inverted version of the escapement cam originally developed by Leonardo da Vinci [5]. The cam features a logarithmic spiral profile that reduces the force exerted by the compression of a spring, therefore reducing the required motor

torque. These phenomena are a result of the cam featuring a linear decrease in the radius as the follower travels along the cam's profile. Shown in Equation 4.1 is the polar representation that describes the cam's profile,

$$r(\theta) = R_i \exp\left(\frac{\log \frac{R_o}{R_i}}{2\pi} \theta\right) \quad (4.1)$$

where R_i and R_o are the inner and outer radii of the cam, respectively, θ is the rotation angle, and $r(\theta)$ describes how the radius of the profile changes as a function of θ .

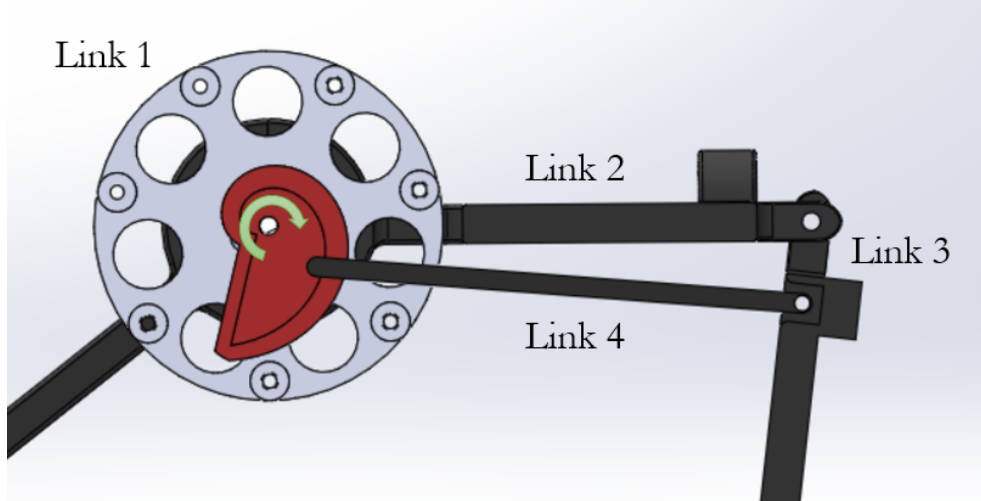


Figure 4.1: Escapement cam attached to four-bar linkage. The green arrow represents the direction of the cam's rotation.

Figure 4.1 shows how an escapement cam is utilized with a four-bar linkage to place the cam and motor at the center of the robot's body. This placement allows for the bulk of the actuator mass to be concentrated at the center of the robot, which is the desired placement for the overall center of mass. The escapement cam's four-bar

linkage is formed as follows:

- Link 1 is the ground link and is formed by the body of the robot.
- Link 2 is the rear leg support and is rigidly attached to link 1.
- Link 3 is attached to link 2 by a pin joint and contains a torsional spring.
- Link 4 is formed by the follower and is essentially a pin and slot joint.

The cam travels in a clockwise motion when the motor is actuated. This motion causes the follower to travel linearly toward the center of the cam's rotation, resulting in the compression of the spring between links 2 and 3. Once the follower reaches the inner radius of the cam, the escapement mechanism is reached and the follower travels rapidly back to the outer radius, releasing the energy stored in the spring.

Determining how much torque is required by the motor to compress the spring is the primary concern for development of this mechanism. The torque required for the motor to turn the cam mechanism is dependent on three factors: the force required to compress the spring, the amount of mechanical advantage provided by link 3, and the amount of frictional force created between the cam and follower. The first two factors resulted in a design trade-off that needed iteration to achieve optimal parameters. After parameters were developed, the torque acting on the motor was calculated.

The length of link 3 determines its mechanical advantage and how much force is required to compress the torsional spring. From a simple moment balance the longer link 3 is, the less force the cam will experience from link 4. However, increasing the

length of link 3 requires a larger difference between the cam's maximum and minimum radii to sweep the rear leg through the desired angle of 150 degrees. A larger change in radius requires an increase in the overall size of the robot. If link 2 becomes too short, the size of the motor must be increased to compensate for a larger force applied on the cam. Increased motor size results in greater robot weight. To solve the design trade-off, one of the parameters was fixed and then iterated to determine the proper cam for the robot.

The most crucial parameter is the cam's size because it dictates the robot's overall size. To determine the cam size parameter, the maximum desired robot size was used. Further constraints on the cam housing size were a result of constraints developed for the front leg design, which will be presented in more detail in Section 4.4. Considering these constraints, the maximum outer radius of the cam was determined to be 19 mm. The inner radius was determined by the minimum size of commercially available bearings for the follower, which had an inner radius of 1.59 mm. These two parameters subtracted from one another determine the amount of linear motion the cam is able to produce.

Determination of linear displacement achievable by link 4 allows for calculation of how much mechanical advantage link 3 provides, and the resulting force the cam will experience from compression of the torsional spring. The attachment point of link 4 can be established by approximating the linear motion of link 4 as the arc length created by link 3 where the two links meet. The attachment point is analogous to the radius of the arc formed between link 3 and the pin joint between links 2 and 3.

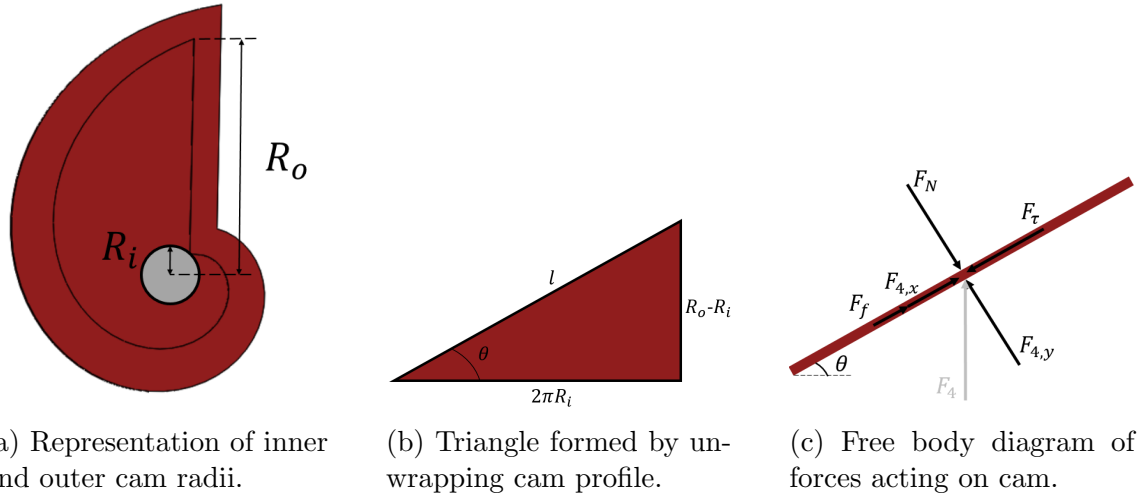
We calculated the radius r using Equation 4.2,

$$r = \frac{s}{\theta} \quad (4.2)$$

where θ is the sweep angle in radians and s is the arch length. The resulting placement of link 4 onto link 3 was determined to be at a radius of 13.34 mm.

The cam will need to overcome friction forces, which are a result of contact friction on the follower in three places: the cam's profile, the cam's face, and the inner wall of the cam housing. Frictional forces are difficult to characterize, therefore steps were taken to reduce their effects at these points. The point where the follower contacts the cam's profile was created out of a stainless steel shaft and mounted on two bearings. The use of two bearings, and the 3:5 diameter shaft rule was followed [26], to compensate for the moment created from the shaft's contact with the cam. The follower only contacts the cam's face when approaching the inner radius. Consequently, this point is where force from the spring's compression has the least effect on motor torque and is negligible compared to the torque required to turn the cam when the follower is at the maximum radius. To mitigate the frictional force where the follower contacts the inner wall of the cam's cage, two dissimilar materials were used: ABS plastic and aluminum.

A method was adopted from work done by Carbiener [25] to calculate the amount



(a) Representation of inner and outer cam radii.
(b) Triangle formed by unwrapping cam profile.
(c) Free body diagram of forces acting on cam.

Figure 4.2: Exploitation of cam's geometry to determine forces acting on the cam's profile [25].

of input torque required to turn the cam. Carbiener's method approximates the force the follower exerts on the cam into a point force, and then utilizes the cam's geometry to determine how much force the cam experiences. This force, coupled with the follower's position from the center of the cam's rotation, allows for the determination of how much torque will be required to turn the cam. As in Section 4.1, the follower experiences a constant decrease in radius as it travels around the cam's profile, which is analogous to the follower traveling up a right triangle slope. To determine slope, we calculated the base and height of the triangle. The base of the triangle is defined by the circumference of the circle, which forms the inner radius R_i , defined in Figure 4.2a. The height of the triangle is the difference in the radial distance the follower travels, which is defined as the outer radius of the cam R_o and R_i . The resulting right triangle is depicted in Figure 4.2b. With geometry defined, a free body diagram was

constructed to determine the amount of force the follower exerts on the cam. The free body diagram is shown in Figure 4.2c, where F_4 is the force exerted by the follower, F_N is the resulting normal force, F_f is the friction force, and F_τ is the force the cam must overcome to rotate. Finally, the maximum required input torque τ_{max} is when the follower is at R_o and can be determined using the relationship shown in Equation 4.3.

$$\begin{aligned}\tau &= r * F_{s,t}(r) \\ \tau_{max} &\geq R_o * F_{s,t}(R_o)\end{aligned}\tag{4.3}$$

The required amount of motor torque was calculated by using this relationship, along with the required spring energy from Chapter 2, and the placement of link 4 from Section 4.1.

4.2 Motor and Controller

After design parameters for the jumping mechanism were determined, a motor controller, and power supply were selected to drive the system. The selection of the motor identified the power requirements, and subsequently defined the battery and motor driver requirements. After identifying these components, we selected a microcontroller and wireless communication method.

In addition to overcoming the required input torque, the motor had to be small, lightweight, and commercially available. The Pololu 1000:1 Micro Gearmotor HP was selected to satisfy all of these requirements. The chosen motor features a 0.883 Nm stall torque at 1.6 A, a weight of 10.5 g, and a compact form factor.

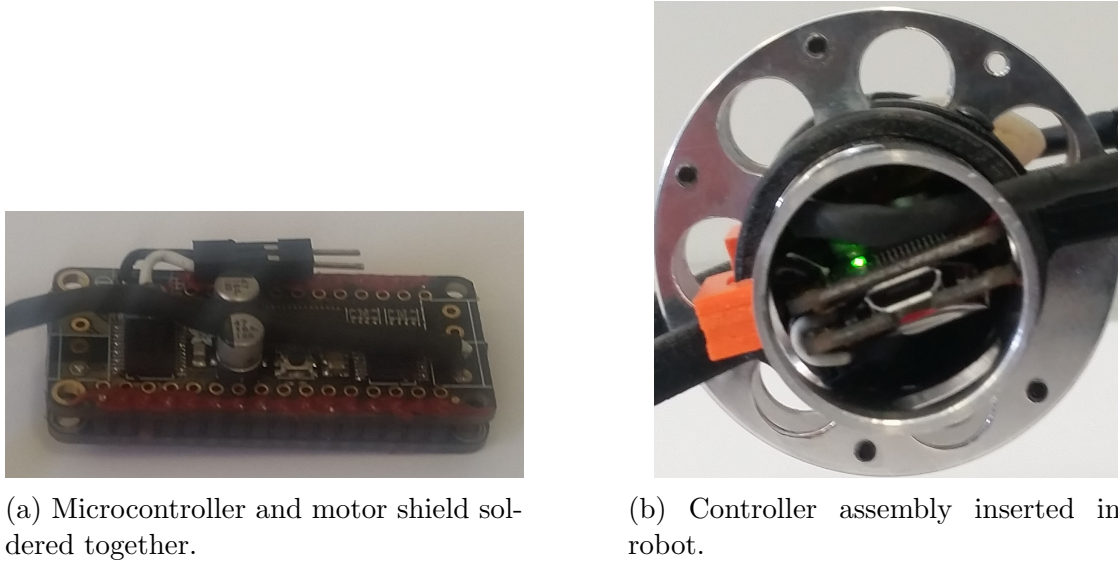


Figure 4.3: Implementation of microcontroller and motor shield.

We implemented a microcontroller to control the robot. The design criteria for the controller were being lightweight, and able to send and receive signals wirelessly. We selected the Adafruit Feather 32u4 Bluefruit LE microcontroller. Bluetooth communication capabilities allow the robot to be controlled and reprogrammed remotely. A drawback to using this controller is any current output over 500 mA can cause damage.

We used a motor driver to overcome the current limits of the microcontroller. We selected the Adafruit DC Motor FeatherWing motor driver, which features a maximum current output of 3.2 A. The benefits of using this driver are that it is designed to mount directly to the microcontroller, and features easily programmable libraries. The microcontroller and motor driver were soldered together to achieve a compact form-factor, and inserted inside the main body of the robot, see Figure 4.3.

The final design requirement was to determine a power supply for the controller and motor driver. We selected two lithium-ion batteries as power supplies. The batteries produce 3.7 V and have a maximum discharge rate of 500 mA. The discharge rate is below the maximum current required for the motor to operate at peak torque. However, physical testing of the motor with an external power supply and multimeter shows that under normal operation the current draw does not exceed 350 mA when connected to the cam.

4.3 Mass Concentration

The goal in jumping robot design is to make the robot as lightweight as possible, which reduces the amount of force required to lift the robot off the ground and achieve the maximum possible jump height. For our robot, the most crucial design constraint for the weight was ensuring the center of mass was concentrated along the center of the robot's body. Furthermore, the legs of the robot needed to be essentially massless compared to the rest of the body, since their mass was not considered in the modeling done in Chapter 2.

To satisfy these constraints the main body was created as a symmetric cylinder about the X axis and was offset along the YZ plane, shown in Figure 4.4. The cylinder design was chosen to allow for a hollow cavity to house the motor and controller, and to minimize the space required to protect the cam mechanism. Section 4.4 will show how the cylindrical shape also provides an ideal surface for ensuring that the robot is able to perform vaulting jumps. Table 4.1 listing weight distribution, shows

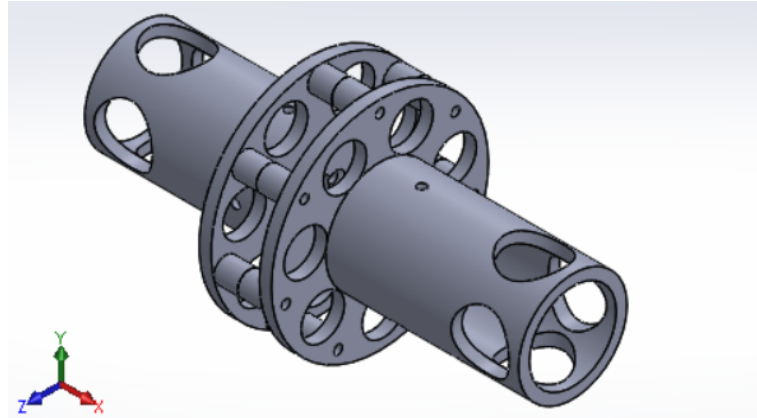


Figure 4.4: CAD model of robot's main body.

the controller and batteries outweigh the motor and cam mechanism. The weight imbalance resulted in a need to place the motor further from the axial center of the cylinder. To help balance the weight distribution, the batteries were placed as close to the axial center as possible.

Table 4.1: Weight distribution for jumping robot.

Part Name	Weight (g)
Body	59.2
Front Legs	14.6
Rear Leg	21.7
Follower	2.5
Controller	15.2
Motor	10.5
Batteries	7.6
Cam	2.9
Hardware	4.9

Balancing the weight about the X axis was difficult to address. Without the addition of extra weight, a plausible method for actuator and cam weight balance

does not exist. Without balance, the robot experiences a negative rotation about the X axis during a jump. This will be further discussed in Chapter 6.

4.4 Vaulting Mechanism

The vaulting mechanism refers to the joint between links 3 and 4. The angle between these links dictates the robot's jumping behavior. This joint's design criteria requires it to behave as a friction free pin joint with angular constraints restricting the angle θ to between 115 degrees for the aiming jump, and 180 degrees for the vaulting jump. This joint is important because the front leg's center of rotation needs to be coincident with the center of mass, which is located at this joint.

The first determination in design of this joint was how to ensure the front legs are able to rotate around the robot's center of mass, while sweeping the angle θ , without any restriction from other parts of the robot. To accomplish this, we built two separate front legs and connected them with a cross bar at mid-length, to ensure even tracking. The legs were designed to feature large, open, cylinders at the top where they interface with the cylindrical main body. The interface was designed to allow the legs to fit concentrically with the cylindrical body, while remaining large enough to fit around the outside. This design allows the front legs to pivot freely around the entire robot until they reach the rear leg. The body and front legs needed to be constructed of two different materials, to ensure this joint was as friction free as possible. Aluminum was selected for the main body due to its rigidity, weight, and cost. The front legs were constructed of ABS plastic to ensure they would be

relatively weightless compared to the main body, and were easy to manufacture using 3D printing methods.

We preformed static stress analysis to ensure the leg design had sufficient strength to support the force applied by the spring. Our analysis determined the necked-down portion of the rear leg was the weakest point. The following Equations 4.4 were used to calculate the maximum sheer stress σ_{max} and normal stress τ_{max} .

$$\begin{aligned}\tau_{max} &= \frac{3V}{2A} \\ \sigma_{max} &= \frac{My}{I}\end{aligned}\tag{4.4}$$

where V is the shear force, A is the cross sectional area, M is the bending moment, y is the centroid, and I is the area moment of inertia. Results from the stress calculations show that the maximum sheer and normal stresses the leg experiences are 0.498 MPa and 0.002 MPa, respectively. The normal stress is much larger than the sheer stress, but it is two orders of magnitude lower than the maximum allowable stress of 30.4 MPa. Therefore, the leg design is able to provide sufficient strength for the robot.

The final consideration was to constrain the movement of the front legs to sweep the angles between 115 and 180 degrees. The rotation was constrained by applying hard stoppers, shown in Figure 4.5. We drilled and threaded holes annularly around the body at fifteen degree increments. These holes allow the position of the stoppers to be changed to achieve different jumping behavior. The utilization of stoppers is functional because the robot uses them to rest its front legs before a jump is performed. The stoppers must be manually changed by removing the screws that secure them, and placing them in another position. Actively changing stoppers, either

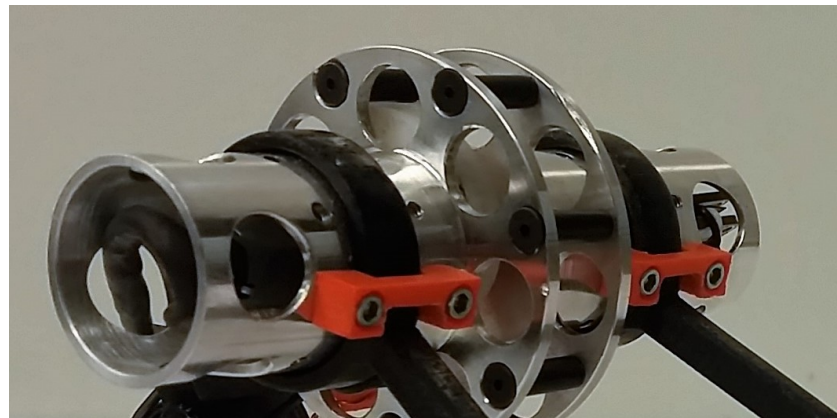


Figure 4.5: Hard stops to constrain the rotation of the robots front legs.

autonomously or remotely, would require the addition of more actuators and may require a redesign of the propulsion mechanism to provide enough power to achieve flight. However, since this robot's primary function is a proof-of-concept, to show different jumping behaviors, and will primarily be used for demonstration purposes, the chosen manual method is sufficient.

Chapter 5: Results and Discussion

To gain insight into the robot's performance, two methods were used to capture its jumping behavior. First, jumps were recorded using a 240 frame per second video camera to visualize the jumping motions. Then we placed the robot into a OptiTrack motion capture system to gather numeric data. The numeric data from the physical model was used to determine jump height, distance, launch angle, and efficiency. We then compared this data to the analytical model which determined if the robot was able to perform as predicted. When jumping, a steel plate is placed in front of the robot to reduce slippage and prevent movement in the front leg's point of contact due to rolling.

5.1 Video Results

The still frame in Figure 5.1 shows the change of the launch angle during the vaulting motion of the jump. This change takes place when the reaction force at the front feet is less than zero. Lack of reaction force at the front feet is evident in the still frame because the front feet have begun to move away from the steel plate. The direction of the initial reaction force is determined before the spring's energy is released, by placing a line through the center of the robot's rear foot, and the center of mass. The initial reaction force is shown by the green arrow on the still frame and is superimposed from

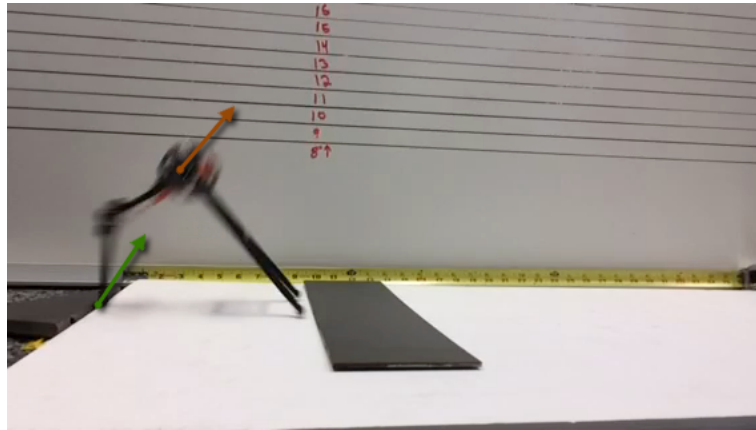


Figure 5.1: Representation of final and initial launch angles for the vaulting jump, shown by the orange and green arrows, respectively.

previous frames of the video. This force provides incite into how much the launch direction changes during the vaulting phase. The direction of the final launch velocity is shown by the orange arrow, which is superimposed from later frames of the video.

Key frames of the two jumps are shown in Figure 5.2. Figure 5.2a shows the aiming jump. The red vectors drawn on the illustrations below the key frames show the reaction force that is experienced by the rear leg. Closer examination shows the robot's main body follows the direction of the reaction force throughout the entire jumping motion. The still frames in Figure 5.2b show the robot performing the vaulting jump. The red arrows in the animation below the key frames, show how the reaction forces change during the jumping motion, as the robot vaults off of its front legs. After the front leg's reaction force becomes zero, the robot's main body then follows the trajectory laid out by the direction of the remaining reaction force at the rear foot. The behavior of these two jumping motions are consistent with previous work done by Faraji et.al [1].

It is apparent in Figure 5.2 that the robot tends to rotate backward as it jumps. The reason for this rotation has to do with the jumping mechanism. When the robot leaves the ground the cam and follower are at their rearmost position on the robot. The weight of the cam, follower, and spring, result in a shift in the center of mass from the axial center of the body. Shifting the center of mass creates a moment causing the robot to rotate backwards. These moments could be countered by adding mass to the front of the robot, however this would add unnecessary weight and is not essential in exhibiting the desired jumping behavior. Also, this trait is desirable for the next step in this project, which will be discussed further in Chapter 6.

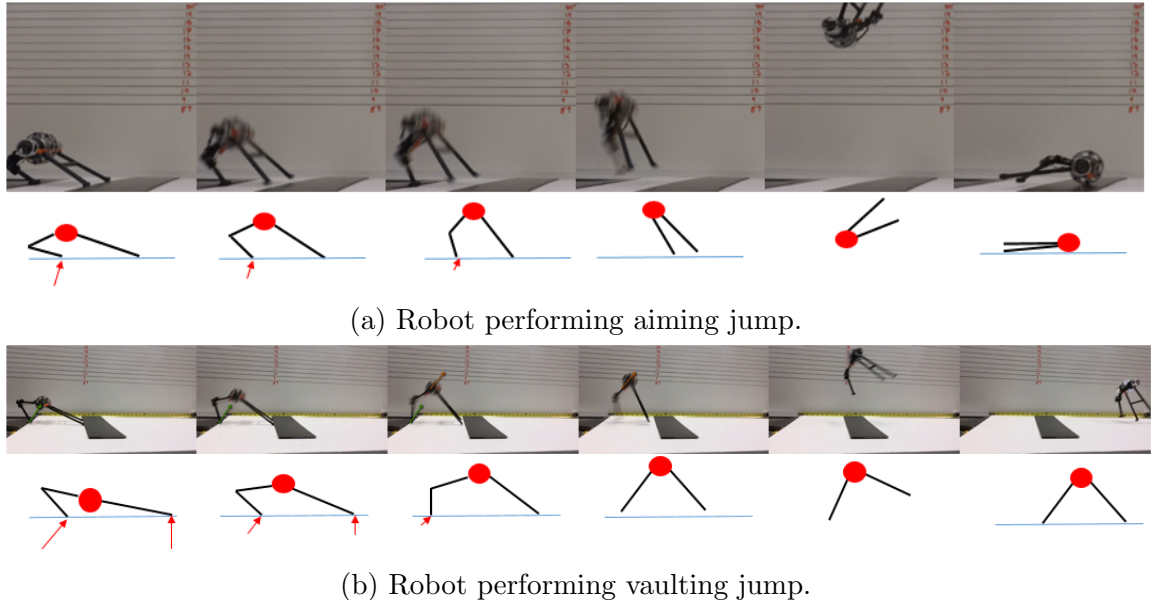


Figure 5.2: Frame by frame shots detailing the robot's behavior as it performs different jumps. The animated representations below photos show how reaction forces effect the robot's jumping behavior.

5.2 Motion Capture

To determine the robot's consistency we recorded ten trials for each jump. The results from these trials are plotted in Figure 5.3. During the aiming jump, the robot reached an average height of 23.6 cm and distance of 18.5 cm, with a maximum standard deviation of 1.37 cm. During the vaulting jump, the robot was able to reach an average height and distance of 17.4 cm and 29.5 cm, respectively, with a standard deviation of 1.55 cm.

An individual trial from both the aiming and vaulting jumps were analyzed to better examine the behavior of the robot during its jumping motion. Individually

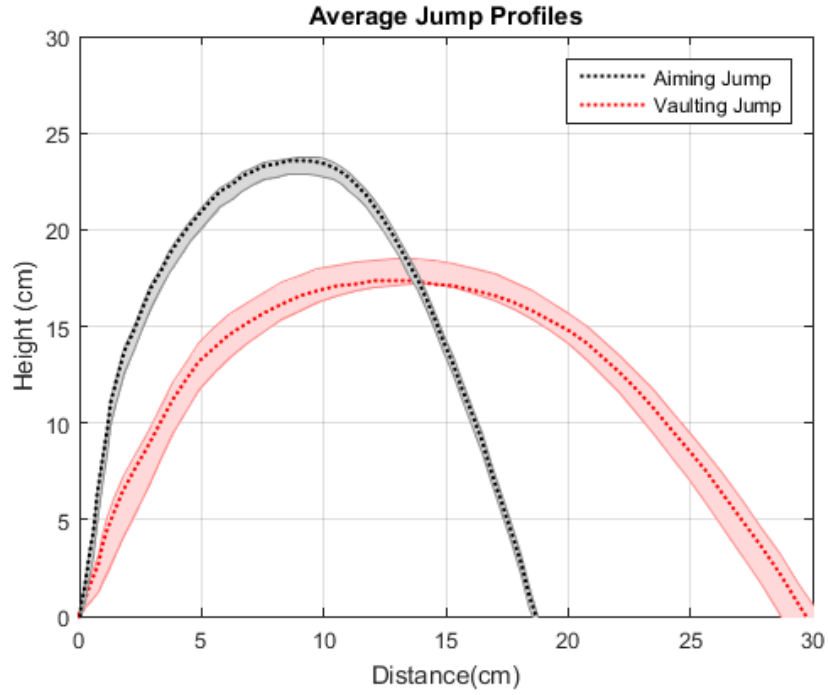


Figure 5.3: Averaged results from motion capture data for the aiming and vaulting jumps.

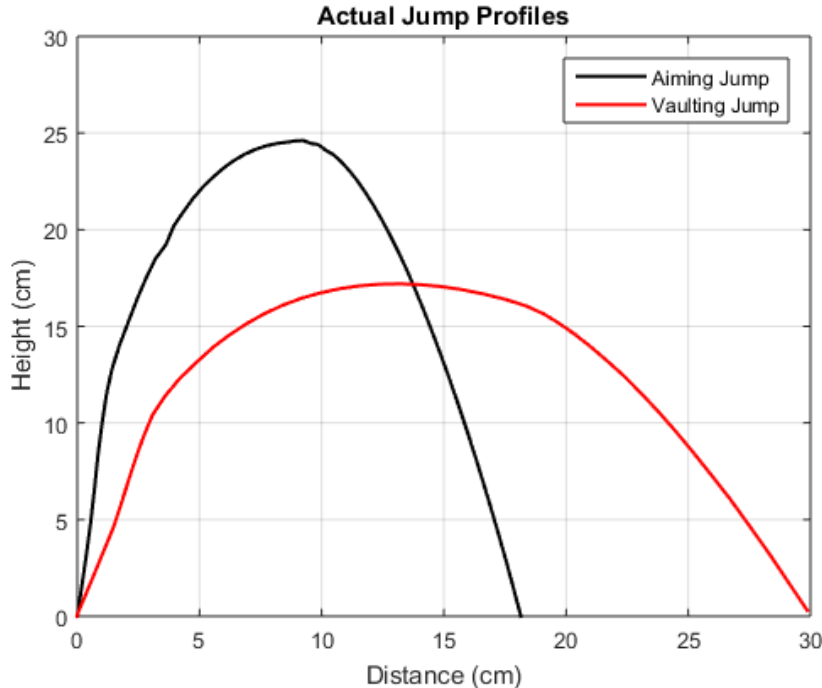


Figure 5.4: Motion capture data from individual iterations of the aiming and vaulting jumps.

analyzing one iteration of the jumps allows us to better determine the launch angle, since it is not skewed like the average. The numeric data for one iteration of each jump is shown in Figure 5.4.

The launch angle for both jumps is consistent with the behavior that was modeled in Chapter 2. The initial launch for the aiming jump is 75.0 degrees and remains constant throughout the jumping motion. For the vaulting jump, the robots initial launch angle is 73.2 degrees before beginning the vaulting motion. Once the vaulting motion is complete, the final launch angle is 52.5 degrees.

A probable explanation for the robot not reaching modeled heights, is due to non-

conservative losses not modeled in the energy balance that was discussed in Chapter 2. The modeled energy methods used, were for the purposes of determining a baseline for the robot's take-off velocity, and allowed for determination of relative performance for the spring selection. The energy balance performed did not account for all losses in the system such as, friction between the feet and the ground, friction at the joints, and work done by the jumping motion. These losses result in less kinetic energy available for the jump.

The shape of the vaulting jump profile is also different than in Chapter 2. This is due to the fact that the modeled behavior assumes that once the spring energy is released, the robot leaves the ground. Analysis of Figure 5.4 shows that the robot is in motion on the ground for the first 10 - 12 cm of the vaulting jump height. It is not until this threshold is reached that the robot begins its parabolic trajectory. During the vaulting motion the robot is losing takeoff velocity resulting in a shorter trajectory.

We preformed power recovery calculations to determine the effectiveness of the propulsion mechanism. Input energy is determined using a load cell to generate a force profile for the spring relative to the angle of the rear leg. With these two parameters the amount of work required to compress the spring can be calculated. Output energy is calculated from the robot's velocity profile during the jumping motion. The robot's velocity is obtained from the motion capture data. Once the velocity is known, the kinetic energy is calculated using the mass of the robot. Power can be calculated from the energy profiles through integration. The resulting input and output powers were determined to be 0.282 W and 2.80 W, respectively, resulting in a power recovery

of 338 percent. The robot is able to exert three times more power than is required to compress the spring. This is a result of the time it takes to store and release the energy. During energy storage the robot takes 5 seconds to compress the spring, which ultimately requires more energy than the robot is able to produce for a jump. However, the spring's energy is released in 0.06 seconds resulting in more power.

Chapter 6: Conclusion

The results obtained in Chapter 5 show the robot developed in this thesis is able to effectively validate the model created by Faraji et.al [1]. The robot's design is based on a four-link mechanism comprised of three pin joints. Jump energy is stored in a torsional spring, which is charged through an escapement cam mechanism. When the escapement point is reached, the springs energy is released and the robot performs a jump. Jumping behavior is dictated by the leg configuration. When the angle between the front and rear legs is at 115 degrees, the springs energy is transmitted directly through the center of mass, resulting in an aiming jump. During an aiming jump the robot follows a trajectory defined by the line formed between the rear foot and the center of mass. When the angle between the front and rear leg is at 180 degrees, some of the spring's energy is transmitted into the front legs, resulting in a vaulting jump. During the vaulting jump, the direction of the rear leg's reaction force changes, until the force at the front legs becomes less than zero. The robot then follows the trajectory dictated by the line formed between the rear foot and center of mass.

Future work for this project involves the development of a more complex model that more accurately represents the autonomy of Salticid spiders. This will be accomplished by developing a more complex three-link mechanism for the rear leg and adding a drag-line to the system. The addition of the more complex leg will allow

for further exploration of jump dynamics in Salticids and help to better understand their jumping mechanics. The addition of a drag-line will allow the robot to further modify its trajectory. This will provide the ability to accomplish trajectories that are not possible through conventional methods. The continuation of the research has the potential to contribute to the development of jumping robots with applications in search and rescue, environmental modeling, and urban warfare.

Bibliography

- [1] H. Faraji, R. Tachella, and R. L. Hatton, “Aiming and vaulting : spider inspired leaping for jumping Robots,” in *IEEE International Conference on Robotics and Automation*, 2016.
- [2] D. E. Hill, “Targeted jumps by salticid spiders (Araneae, Salticidae, Phidippus),” pp. 1–28, 2006.
- [3] R. H. Armour, “A Biologically Inspired Jumping and Rolling Robot,” Ph.D. dissertation, University of Bath, 2010. [Online]. Available: <http://opus.bath.ac.uk/19708/>
- [4] S. Bergbreiter and K. S. J. Pister, “Design of an autonomous jumping microrobot,” in *IEEE International Conference on Robotics and Automation*, no. April, 2007, pp. 447–453.
- [5] U. Scarfogliero, C. Stefanini, and P. Dario, “Design and development of the long-jumping ”grillo” mini robot,” in *Proceedings - IEEE International Conference on Robotics and Automation*, no. April, 2007, pp. 467–472.
- [6] J. Aguilar, A. Lesov, K. Wiesenfeld, and D. I. Goldman, “Lift-off dynamics in a simple jumping robot,” *Physical Review Letters*, vol. 109, no. 17, pp. 1–5, 2012.
- [7] J. Zhang, K. Ding, Y. Zhang, X. Yang, and G. Song, “Modeling and simulation of a bio-inspired symmetrical jumping robot,” in *IEEE International Conference on Mechatronics and Automation*, 2014, pp. 1353–1358. [Online]. Available: <http://ieeexplore.ieee.org/lpdocs/epic03/wrapper.htm?arnumber=6885896>
- [8] J. Zhao, N. Xi, F. J. Cintron, M. W. Mutka, and L. Xiao, “A single motor actuated miniature steerable jumping robot,” in *IEEE/RSJ International Conference on Intelligent Robots and Systems*, 2012, pp. 4274–4275. [Online]. Available: <http://ieeexplore.ieee.org/lpdocs/epic03/wrapper.htm?arnumber=6386293>
- [9] R. Quinn, J. Offi, D. Kingsley, and R. Ritzmann, “Improved mobility through abstracted biological principles,” *IEEE/RSJ International Conference on Intelligent Robots and Systems*, vol. 3, no. October, pp. 2652–2657, 2002.

- [10] C. Yong, “Biological mechanism of the locust jumping robot,” in *International Conference on Electrical and Control Engineering*, 2010, pp. 2676–2679. [Online]. Available: <http://ieeexplore.ieee.org/lpdocs/epic03/wrapper.htm?arnumber=5630623>
- [11] M. Kovač, M. Fuchs, A. Guignard, J. C. Zufferey, and D. Floreano, “A miniature 7g jumping robot,” in *IEEE International Conference on Robotics and Automation*, no. c, 2008, pp. 373–378.
- [12] M. C. Birch, R. D. Quinn, G. Hahm, S. M. Phillips, B. Drennan, A. Fife, H. Verma, and R. D. Beer, “Design of a cricket microrobot,” in *IEEE International Conference on Robotics and Automations*, vol. 2, no. April, 2000, pp. 1109–1114 vol.2.
- [13] J. Yan, T. Wang, X. Zhang, and J. Zhao, “Structual design and dynamic analysis of biological inspired water-jumping robot,” in *IEEE International Conference on Information and Automation*, no. July, 2014, pp. 1295–1299.
- [14] M. Kovač, M. Schlegel, J. C. Zufferey, and D. Floreano, “Steerable miniature jumping robot,” *Autonomous Robots*, vol. 28, no. 3, pp. 295–306, 2010.
- [15] A. Igarashi and S. Mikami, “Frog-like robot with jump and walk mechanism for locomotion on rough terrain,” in *International Conference on Control, Automation, Robotics & Vision*, vol. 2014, no. December, 2014, pp. 3–6.
- [16] M. Noh, S. W. Kim, S. An, J. S. Koh, and K. J. Cho, “Flea-inspired catapult mechanism for miniature jumping robots,” *IEEE Transactions on Robotics*, vol. 28, no. 5, pp. 1007–1018, 2012.
- [17] D. Parry and J. Brown, “The jumping mechanism of salticid spiders,” *The Journal of Experimental Biology*, vol. 36, no. June, pp. 654–466, 1959.
- [18] J. C. Otto and D. E. Hill, “Two new Australian peacock spiders that display inflated and extended spinnerets (Araneae: Salticidae: Euophryinae: Maratus Karsch 1878),” *Peckhamia*, vol. 104, no. 1, pp. 1–28, 2012.
- [19] ——, “Three new Australian peacock spiders (Araneae: Salticidae: Maratus),” *Peckhamia*, vol. 108, no. 1, 2013.
- [20] M. W. Mutka, “Design and testing of a controllable miniature jumping robot,” in *IEEE/RSJ International Conference on Intelligent Robots and Systems*, 2010, pp. 3346–3351.

- [21] J. Zhao, G. Liu, Q. Han, and H. Cai, “A wheeling-hopping combination scout robot,” in *IEEE International Conference on Robotics and Automation*, 2008, pp. 973–981.
- [22] F. Li, G. Bonsignori, U. Scarfogliero, D. Chen, C. Stefanini, W. Liu, P. Dario, and X. Fu, “Jumping mini-robot with bio-inspired legs,” in *International Conference on Robotics and Biometrics*, 2009, pp. 933–938.
- [23] J. Morrey, B. Lambrecht, a.D. Horchler, R. Ritzmann, and R. Quinn, “Highly mobile and robust small quadruped robots,” *Proceedings 2003 IEEE/RSJ International Conference on Intelligent Robots and Systems (IROS 2003) (Cat. No.03CH37453)*, vol. 1, no. October, pp. 0–5, 2003.
- [24] G. Kosa, A. Ayali, T. Aviv, and U. B. Hanan, “Design of a bio-mimetic jumping robot,” in *IEEE Convention of Electrical and Electronics Engineers in Israel*, 2012, pp. 6–8.
- [25] C. P. Carbiener, “Design of a biologically inspired jumping mechanism for a dynamic running platform,” 2014.
- [26] D. H. Slocum, *Precision machine design*. New Jersey, USA: Prentice Hall Inc., 1992.

